

Breakdown of chiral anomaly and emergent phases in Weyl semimetals under orbital magnetic fields

Faruk Abdulla, Anna Keselman, and Daniel Podolsky
*Physics Department, Technion - Israel Institute of Technology, Haifa 32000, Israel and
The Helen Diller Quantum Center, Technion, Haifa 32000, Israel*

An external orbital magnetic field applied perpendicular to the separation vector of a pair of Weyl points can couple them and induce a gap in the electronic spectrum. In this work, we investigate the gap-opening behavior in the presence of a lattice, revealing rich phenomenology absent in the continuum picture. Specifically, we address the emergence of layered Chern insulating states, examining how the anisotropy of the Weyl cone dispersion influences the sequence of phase transitions, and establishing connections to the continuum limit. We analyze the evolution of surface Fermi-arc states across these regimes, highlighting their distinct behaviors during the gap-opening transitions.

I. INTRODUCTION

Weyl semimetals (WSMs) [1–7] represent a robust gapless topological phase of quantum matter in three dimensions. As long as spatial translation symmetry is maintained, the only way to eliminate this phase is by bringing pairs of Weyl nodes (WNs) with opposite chiralities together, allowing them to annihilate each other. WSMs exhibit a variety of exotic phenomena – the chiral anomaly [8–11], chiral anomaly-induced negative magnetoresistance [12–19], planar Hall effect [20–24], Fermi-arc-mediated quantum oscillations, and three-dimensional quantum Hall effect [25–34] – all of which typically rely on the presence of an external orbital magnetic field. However, when the magnetic field strength is sufficiently high, it can couple WNs of opposite chiralities and open a finite gap in the spectrum, thereby destabilizing the WSM state [35–43].

An external magnetic field that is not aligned with the separation direction of WNs can couple nodes of opposite chirality, resulting in the opening of a gap in the bulk electronic spectrum. This phenomenon has been the subject of several theoretical investigations based on low-energy continuum models. Notably, Refs. 40 and 41 demonstrated that the application of an orbital magnetic field immediately induces a gap, which is exponentially small, scaling as $\sim \exp[-(Ql_B)^2]$, where Q represents the momentum-space separation between the Weyl nodes and $l_B = \sqrt{\hbar}/(eB)$ is the magnetic length associated with the applied field. In these models, the gap increases monotonically as the magnetic field strength is raised. Furthermore, Ref. 44 revealed that in systems where the Weyl fermion velocities exhibit anisotropy, the induced gap can display oscillatory behavior as a function of the magnetic field strength, adding further complexity to the field-induced modification of the electronic structure.

It is important to note that these results, derived from continuum approximations, are strictly valid within a specific regime of parameters: when the separation between the Weyl nodes (Q) is much smaller than the linear dimensions of the Brillouin zone (BZ), and when the magnetic length l_B is considerably larger than the lattice constant a , so that lattice effects can be safely ig-

nored. However, these conditions are not always satisfied, particularly under strong magnetic fields where l_B approaches the lattice scale, as in moiré systems, or in materials with relatively large node separations. Similar effects can also arise in two and three dimensional Dirac materials [45] with two or more Dirac cones in the spectrum, e.g. graphene [46, 47], and surfaces of three dimensional topological insulators [48, 49]. In such cases, the low-energy continuum description breaks down, failing to capture crucial lattice-specific phenomena.

Beyond the bulk electronic gap, another significant limitation of the continuum framework is its inability to address the behavior of surface states, specifically the Fermi-arc states, under the influence of magnetic fields. The fate of these topologically protected surface states in the presence of bulk gap openings remains an open and critical question, particularly in understanding the complete topological character of the field-induced gapped phases. Determining whether the gapped state retains a nontrivial topological classification or transitions into a trivial insulating state requires a full lattice-based treatment, beyond the scope of continuum models. Therefore, it is essential to investigate these effects using lattice models capable of capturing both bulk and surface phenomena, as well as the detailed topological structure of the resulting gapped phases.

In this work, we study magnetic field-induced gaps in WSMs in a lattice. We consider the setup depicted in Fig. 1, in which two Weyl cones of opposite chirality are separated by a momentum space distance Q . We assume that both Weyl nodes are at the same energy, which we set to be the Fermi energy. For simplicity, we assume zero tilt in the Weyl cones. A uniform orbital magnetic field is applied in a direction perpendicular to the separation between the Weyl cones.

We find that lattice effects give rise to two important corrections to the previous, continuum-limit, results. First, the discrete translational symmetry of the lattice implies that k -space is periodic i.e. $\mathbf{k} \in \text{BZ}$. Therefore, there are always two separations: Intra-BZ separation which we have already denoted as Q and inter-BZ separation $\vec{Q}' = \vec{G} - \vec{Q}$ (\vec{G} is a reciprocal lattice vector) between two WNs in a lattice. Consequently, there exist

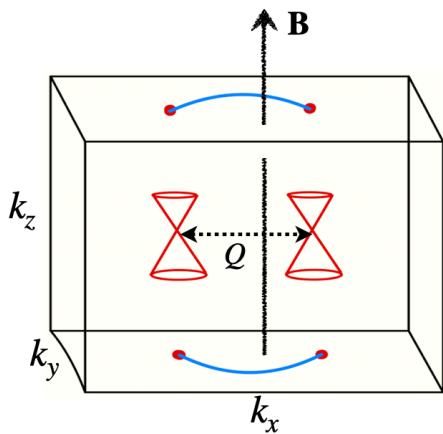


FIG. 1. Schematic of a Weyl semimetal with two Weyl cones placed in a uniform magnetic field $\mathbf{B} \parallel \hat{z}$. Weyl cones are separated along k_x and their momentum space separation is Q . Magnetic field is aligned perpendicular to the direction of separation between Weyl cones of opposite chirality. The orbital field \mathbf{B} introduces a quantum tunneling of particles between the Weyl cones which can induce a finite gap in the spectrum. A schematic phase diagram is depicted in Fig. 2.

two distinct ways of gap opening induced by the orbital magnetic fields and hence we expect two topologically distinct gapped states. Second, the Landau levels (LLs) are not perfectly flat. They acquire a finite dispersion which is significant in the Hofstadter regime $l_B \sim a$. These dispersive LL bands can alter the gap structure in the system. The objective of this paper is to provide a comprehensive understanding of these phenomena. We will initially review the continuum description, followed by a detailed investigation of lattice effects.

The paper is organized as follows. In Section II we present a summary of our main results. In Section III, we revisit the low-energy continuum description of gap opening induced by an orbital magnetic field. As we mentioned before, Ref. 40 found the gap to be monotonic with the field, whereas Ref. 44 found the gap can exhibit periodic oscillations. In this section, we provide a unified description of the phenomena to set the stage for the richer phenomenology in a lattice description. The analysis in the presence of a lattice is carried out in Section IV, which contains the main results of this work. We conclude in Section V.

II. MODEL AND SUMMARY OF THE RESULTS

We consider a minimal two-band model of WSM with two WNs which breaks time-reversal but preserves inversion. We assume a cubic lattice model with the WNs located on the k_x axis at $k_x = \pm k_0$, with the Hamiltonian

$$H(\mathbf{k}) = 2\tilde{v}_x m(\mathbf{k})\sigma_x + 2v_y \sin(k_y a)\sigma_y + 2v_z \sin(k_z a)\sigma_z, \quad (1)$$

where $m(\mathbf{k}) = 2t^2 + (\cos k_0 a - \cos k_x a) - t^2(\cos k_y a + \cos k_z a)$, $\tilde{v}_x = v_x/\sin k_0 a$, and a is the lattice constant (we will often work in units in which $a = 1$). Here, $\sigma_{x,y,z}$ are Pauli matrices. The parameter k_0 , which sets a separation of $Q = 2k_0$ between the Weyl cones, lies in the range $0 < k_0 < \pi/a$. In general, the term $m_0(\mathbf{k})\sigma_0$ is allowed in the above Hamiltonian (inversion symmetry $P = \sigma_x$ constrains $m_0(\mathbf{k})$ to be an even function of momentum). It introduces a tilt to the Weyl cone and also shifts the WNs in energy and can have significant effect on the magnetic field induced gaps. In what follows we will ignore this term and focus on the relatively simple but still phenomenologically rich situation described by the Hamiltonian in Eq. (1). In the following, we will assume magnetic field is aligned along the z direction and work in the Landau gauge $\mathbf{A} = (-y, 0, 0)B$, unless explicitly stated otherwise.

The setup is depicted in Figure 1. For a field along the z direction, the momentum along \hat{z} remains conserved and we can set it to $k_z = 0$, since our focus is on low-energy properties. The key parameters in the problem are the momentum-space separation between the Weyl cones, Q , the velocity components (v_x, v_y) of the Weyl fermion perpendicular to the magnetic field and the parameter t . From these we define a single parameter

$$\gamma = \left(1 - \frac{1}{t^2} \frac{v_y^2}{v_x^2}\right) \quad (2)$$

which captures the anisotropy of the Weyl cone dispersion and controls the distinct behaviors of the induced gap. This parameter will play a crucial role in the subsequent analysis. The sign of γ determines the shape of the Fermi pockets around the Weyl nodes, which are elliptical for $\gamma < 0$ and crescent-shaped for $\gamma > 0$, as shown in Fig. 2.

We find that an orbital magnetic field perpendicular to the direction of separation between Weyl cones introduces a tunneling of electrons between them, thus inducing a gap in the electronic spectrum. The gap is non-perturbative with the magnetic field i.e. it is exponentially small in the field and becomes significant when $\sqrt{v_x/v_y} l_B \sin k_0 a \sim 1$. Depending on the anisotropy in the Weyl cone dispersion, the behavior of the induced gap alters significantly. There are two distinct regimes which are distinguished by the anisotropy parameter γ , defined in Eq. 2. Here we summarize the results in the case $\phi_B \ll \phi_0$ i.e. the flux through a 2D unit cell of area a^2 is much smaller than the flux quantum $\phi_0 = h/e$, which is the relevant regime in typical experiments. In later sections, we will also discuss the very large field regime ($\phi_B \sim \phi_0$).

(i) For $\gamma < 0$, the system displays three phases as a function of the separation between the Weyl nodes, Q , see Fig. 2(a3). For small Q , the system is a normal insulator (NI), whereas for large Q it is a layered Chern insulator (LCI). The LCI phase can be viewed as a collection of two-dimensional Chern insulators stacked along

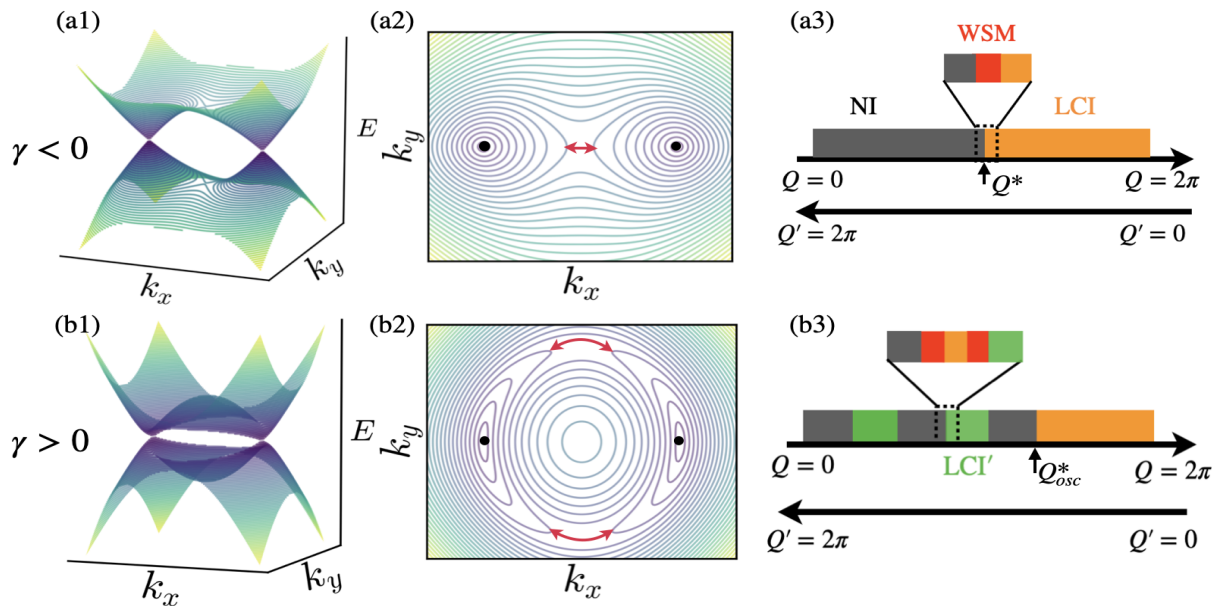


FIG. 2. Band structures for $\gamma < 0$ and $\gamma > 0$ are shown in (a1) and (b1) respectively. (a2)-(b2) Constant energy contours around the Weyl nodes have elliptical and crescent shape for $\gamma < 0$ and $\gamma > 0$ respectively. Weyl nodes are represented by black dots. There is only a single close encounter for $\gamma < 0$, and two close encounters for $\gamma > 0$ between the Fermi pockets around the Weyl nodes. (a3)-(b3) Schematic phase diagram (for a system on a lattice) in presence of an orbital magnetic field $\mathbf{B} \parallel \hat{z}$ which is perpendicular to the direction of separation between two Weyl nodes of opposite chirality. Here Q and Q' represent the intra and inter BZ separation between the Weyl nodes in momentum space. (a3) For $\gamma < 0$, the system displays three phases as a function of the separation between the Weyl nodes Q . The transition from normal insulator (NI) to layered Chern insulator (LCI) passes through a gapless WSM phase. The width of the WSM region is exponentially small in ϕ_B^{-1} . (b3) For $\gamma > 0$ and a fixed applied flux, there is a series of phase transitions as we tune the separation $Q \in (0, 2\pi)$. Besides NI and LCI, another insulating state which we denote as LCI' appears. The state LCI' can be viewed as two copies of LCI with opposite Chern numbers. All transitions between NI and LCI' phases pass through a sequence of three phases: two WSMs and an LCI.

the x direction, hosting chiral surface states on surfaces that result from termination along the y and z directions.

We denote the critical momentum space separation at which the transition occurs by Q^* . These two insulating phases are separated by a gapless WSM phase. The width (range of Q values) of the WSM region is exponentially small in ϕ_B^{-1} . This is associated with the finite bandwidth of the LLs which is exponentially small in ϕ_B^{-1} . For fixed Q inside the insulating phases, the gap increases monotonically with the field.

(ii) For $\gamma > 0$, as Q is increased from zero, the system alternates between NI and a distinct insulating phase, which we denote LCI', and which can be viewed as two copies of LCI with opposite Chern numbers. LCI' is a symmetry-protected topological phase relying on translational and mirror symmetries – in their absence, the phase is indistinguishable from NI. This alternation continues until Q reaches a value Q_{osc}^* , beyond which the system enters an LCI state, see Fig. 2(b3). The transitions between NI and LCI' phases are separated by finite-size regions (that are exponentially narrow in ϕ_B^{-1}) consisting of three phases: two WSM states which are separated by a gapped LCI state. For fixed $Q < Q_{osc}^*$, the induced gap oscillates with the applied field and vanishes in an almost periodic manner (strictly periodic in the contin-

uum). The envelope of oscillations decays exponentially with $(Ql_B)^2$.

It is worth emphasizing which of these effects rely on the presence of a lattice. First of all, the appearance of an LCI phase at large Q (for either case) is directly attributed to the periodic nature of the BZ. In addition, the appearance of WSM (for $\gamma < 0$) and WSM-LCI-WSM regions (for $\gamma > 0$) separating the insulating phases only occurs on a lattice, where the LLs develop a dispersion in momenta perpendicular to the direction of the field. Finally, the identification of the topological nature of the LCI and LCI' phases is only possible in a lattice model.

In addition, the fact that we work with a lattice model enables us to make a systematic study of the fate of the Fermi-arc states in the presence of commensurate magnetic fields. For the case $\gamma < 0$, we find that the Fermi-arc states are either immediately gapped out or evolve to a Fermi loop which extends to the edges of the surface BZ. For $\gamma > 0$, the situation is more involved because of the oscillations and periodic appearance of the WSM state. However in either case, the fate of Fermi-arc surface states can be predicted from the topology of the bulk states, as will be discussed below.

III. CONTINUUM DESCRIPTION

In this Section, we present a unified description of the low-energy continuum behavior of our model, previously discussed in Refs. [38, 40, 44].

A single Weyl fermion centered at momentum $\mathbf{Q}/2$ is described by the Weyl Hamiltonian, $H(\mathbf{k}) = \sum_i v_i (k_i - Q_i/2)\sigma_i$, where $\mathbf{v} = (v_x, v_y, v_z)$ is the velocity. In the presence of a quantizing orbital magnetic field, $\mathbf{B} \parallel \hat{z}$, the spectrum consists of graphene-like LLs $E_n = \pm \sqrt{\frac{2|v_x v_y|}{l_B^2} n + v_z^2 k_z^2}$ ($n = 1, 2, \dots$). In addition, the spectrum contains a special chiral LL which disperses linearly in momentum along the direction of the field, $E_0 = \eta v_z k_z$, with $\eta = \text{sgn}(v_x v_y v_z)$ the chirality of the Weyl fermion. The gapless chiral LL is responsible for phenomena associated with chiral anomaly physics, including negative magneto-resistance, thickness-dependent quantum oscillations, and 3D quantum Hall effect in Weyl semimetals.

In WSMs, Weyl fermions always come in pairs of opposite chirality, separated by a finite distance Q in momentum space, and by a finite energy barrier. This gives a correction to the low energy spectrum due to the tunneling of electrons from one WN to the other. This correction is exponentially small in $Q l_B$ and hence nonperturbative in field. The effect will be significant when the cyclotron gap $\sqrt{2|v_x v_y|}/l_B$ is comparable to the height of the barrier, which can be approximated by $v_x Q/2$ assuming that the WNs are separated in the k_x direction. Therefore the condition for states around the two WNs to be strongly coupled can be expressed as

$$\sqrt{\left| \frac{v_x}{v_y} \right|} Q l_B \lesssim 1, \quad (3)$$

which depends on the anisotropy of the Weyl cone. The above condition was derived before in Ref. 38.

The condition for chiral LLs of two Weyl nodes to be strongly coupled can also be stated in terms of the overlap of their wavefunction in momentum space. In the Landau gauge, $\mathbf{A} = (-y, 0, 0)B$, the wavefunction of the chiral LL associated with a Weyl node at $\pm \mathbf{Q}/2$ is $|ZLL\rangle \sim \exp\left(-\left|\frac{v_x}{v_y}\right| \frac{l_B^2}{2} (k_x + y/l_B^2 \mp Q/2)^2\right)$. The overlap of these two wavefunctions is $\propto \exp\left(-\left|\frac{v_x}{v_y}\right| \frac{l_B^2}{4} Q^2\right)$ and becomes significant when $\sqrt{|v_x/v_y|} Q l_B \lesssim 1$, which is identical to the condition in Eq. 3.

The preceding discussion gives only a qualitative picture of coupling of two WNs and the potential gap opening in the spectrum in presence of an orbital magnetic field directed perpendicular to their separation. Below we consider a low-energy model of WSM and discuss quantitatively how the field-induced energy gap behaves with the magnetic field and the anisotropy parameter γ .

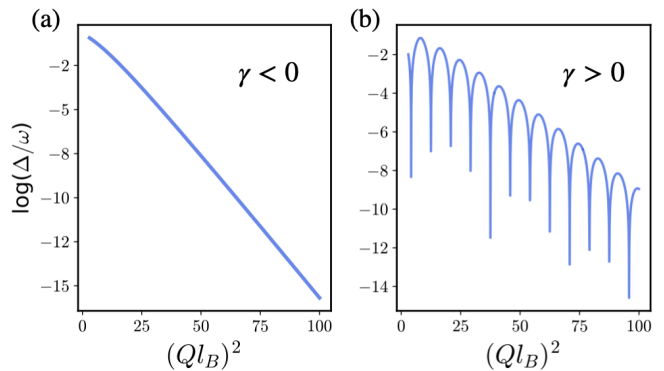


FIG. 3. Energy gap (Δ) in the continuum model as a function of the square of the dimensionless parameter Ql_B , computed numerically for $t = 1$. (a) For $\gamma = -0.44$, the field-induced gap falls exponentially with Ql_B . (b) For $\gamma = 0.96$, the gap oscillates and periodically goes to zero (at the troughs). The troughs in the figure are not exactly at zero because of the finite line grid in the numerical computation. Here the envelope of oscillations falls exponentially.

A. Low energy continuum model

When the separation $Q = 2k_0$ between the Weyl cones is small compared to the linear dimension of the BZ, the lattice Hamiltonian (Eq. 1) can be approximated to

$$H(\mathbf{k}) = \tilde{v}_x m(\mathbf{k}) \sigma_x + 2v_y k_y \sigma_y + 2v_z k_z \sigma_z, \quad (4)$$

where now $m(\mathbf{k}) = (k_x^2 - k_0^2) + t^2(k_y^2 + k_z^2)$, and $\tilde{v}_x = v_x/k_0$. For a field along the z direction, momentum along z remains conserved. We are interested in the energy gap at the band bottom $k_z = 0$.

As we have already mentioned, the anisotropy parameter γ (defined in Eq. 2) controls the structure of the gap as a function of Ql_B . For an arbitrary t , the problem of computing the gap analytically becomes challenging because one would require solving a fourth-order differential equation. However, as shown in Ref. 44, a wealth of information on how the induced gap behaves as a function of magnetic flux or WN separation can be extracted analytically without solving the full eigenvalue problem.

B. Zero energy solutions

Following Ref. 44 it is possible to obtain analytic conditions for the system to remain gapless, even in the presence of a magnetic field. The authors in Ref. 44 considered the case of $t = 1$. Here we generalize the treatment to arbitrary $t \neq 0$ (the case $t = 0$ is discussed in detail below).

For an orbital magnetic field along z direction and in the gauge $\mathbf{A} = (-y, 0, 0)B$, the momenta k_x and k_z remain good quantum numbers. External magnetic field is introduced via minimal coupling $k_x \rightarrow (k_x + y/l_B^2)$. Introducing the ladder operators $a = \frac{l_B}{\sqrt{2t}}(k + \frac{t}{l_B} \frac{d}{dk})$,

$a^\dagger = \frac{l_B}{\sqrt{2t}}(k - \frac{t}{l_B^2} \frac{d}{dk})$, where $k = (k_x + y/l_B^2)$, the Hamiltonian in the presence of a magnetic field can be expressed as

$$H_\phi = \omega \begin{pmatrix} 0 & h^\dagger \\ h & 0 \end{pmatrix} \quad (5)$$

where $h = [a^\dagger a - \delta + \eta(a - a^\dagger)]$, $\delta = \frac{k_0^2 l_B^2}{2t} - \frac{1}{2}$, $\eta = \frac{k_0 l_B}{\sqrt{2t^3}} \frac{v_y}{v_x}$, and $\omega = \frac{2v_x t}{k_0 l_B^2}$. Note that $H_\phi^2 = \omega^2 \begin{pmatrix} h^\dagger h & 0 \\ 0 & h h^\dagger \end{pmatrix}$. Hence, H_ϕ has a zero-energy eigenvalue if and only if h has a zero eigenvalue. The eigenvalues of h are

$$\lambda_N = N + \frac{1}{2} - \frac{k_0^2 l_B^2}{2t} \gamma, \quad (6)$$

where $N = 0, 1, 2, \dots$, and $\gamma = (1 - v_y^2/(v_x^2 t^2))$ as defined in Eq. (2).

Clearly, the spectrum does not contain zero-energy eigenvalues when γ is negative. In this case, the spectrum is always gapped for any finite values of magnetic field. On the other hand, for positive γ , zero-energy eigenvalues occur periodically in $k_0^2 l_B^2$ at the values $\gamma k_0^2 l_B^2 = t(2N + 1)$. Therefore, the gap closes periodically with $(k_0 l_B)^2$. The period of oscillation in l_B^2 is $T l_B^2 = \frac{2\pi}{\gamma A}$, where

$$A = \pi k_0^2 / t. \quad (7)$$

For $v_y = 0$, the model in Eq. 4 describes a nodal loop semimetal and then A is the area of the nodal loop $k_x^2 + t^2 k_y^2 = k_0^2$.

C. Structure of the induced gap

To find the behavior of the energy gap Δ as a function of field and WN separation Q , we numerically diagonalize the Hamiltonian in Eq. 5 in a LL basis by truncating to a hundred Landau levels. We notice that the separation parameter $k_0 = Q/2$ and magnetic length l_B always appear as a dimensionless product $k_0 l_B$ in the block h . Therefore the spectrum and energy gap of H_ϕ/ω are functions of the dimensionless parameter $Q l_B$. The numerically computed energy gap Δ is plotted in Fig. 3. We find that Δ/ω decays exponentially in $(Q l_B)^2$. For $\gamma < 0$, this decay is monotonic and the gap never closes. By contrast, for $\gamma > 0$, the gap vanishes periodically with $(Q l_B)^2$, in agreement with the results of Sec. III B.

We can understand the monotonic regime from the special case $t = 0$, which was studied in Ref. [40]. Note that for $t = 0$, the anisotropy parameter γ is always negative for any finite value of the ratio v_y/v_x . For $t = 0$, the problem of finding the spectrum in a uniform magnetic field along z can be mapped to a Schrodinger equation with an asymmetric double-well potential. The authors in Ref. [40] found that the induced gap is nonperturbative in magnetic field. They computed the energy gap

(Δ) using the WKB approximation and found it to be exponentially small in $Q l_B$:

$$\Delta \approx \frac{v_x}{\sqrt{\pi}} \sqrt{\frac{v_x}{v_y}} \frac{1}{l_B} e^{-\frac{1}{6} \frac{v_x}{v_y} (Q l_B)^2}. \quad (8)$$

The orbital magnetic field immediately introduces a finite gap in the electronic spectrum (i.e. gapping the WNs) which increases monotonically with $B \propto 1/l_B^2$. We note that the gap Δ is significant only when the condition (3) is satisfied.

D. Discussion

Several comments are in order. The oscillation and the periodic closing of the energy gap cannot be understood from the Onsager theory; its origin is purely a quantum phenomenon. The Fermi surface at zero energy consists only of two isolated points- the two Weyl nodes. At energies away from the energy of WNs, the Fermi surface consists of two disjoint and identical Fermi pockets around the Weyl nodes in the k_x - k_y plane. When an orbital magnetic field is applied it induces a quantum tunneling from one Fermi pocket to the other, a phenomenon known as magnetic breakdown [50–52]. It is this quantum tunneling between the two Fermi pockets around the WNs which leads to a gap opening in the spectrum. The probability of tunneling is exponentially small in the distance between the Fermi pockets and the height of the barrier, giving rise to the exponential decay in $(Q l_B)^2$. For $\gamma > 0$ the Fermi pockets are in crescent shape with two close encounters as shown in Fig. 2(b2). This gives two possible tunneling paths for the magnetic breakdown. The interference between these gives rise to the periodic gap closings. The area enclosed by the two paths is A as defined in Eq. (7) accounting for the period of oscillations. Note that this picture relies on mirror symmetry which ensures that the two tunneling paths have exactly the same amplitude. If the symmetry were absent, the destructive interference would be imperfect, and the periodic gap closings would not occur. On the other hand for $\gamma < 0$ the Fermi pockets have an elliptical shape as shown in Fig. 2(a2) with only one close encounter between them, leading to a monotonic behavior of the gap.

The continuum calculation provides a good description only when the separation Q between the WNs is much smaller than the linear dimension of the BZ i.e. $Q \ll \pi/a$ and for $l_B \gg a$. We devote following sections to study the effects of the lattice.

IV. TOPOLOGICAL NATURE OF THE GAPPED PHASES ON A LATTICE

The lattice model allows us to discuss the topological nature of the gapped phases induced by orbital magnetic fields. It is instructive to start from the Weyl semimetal

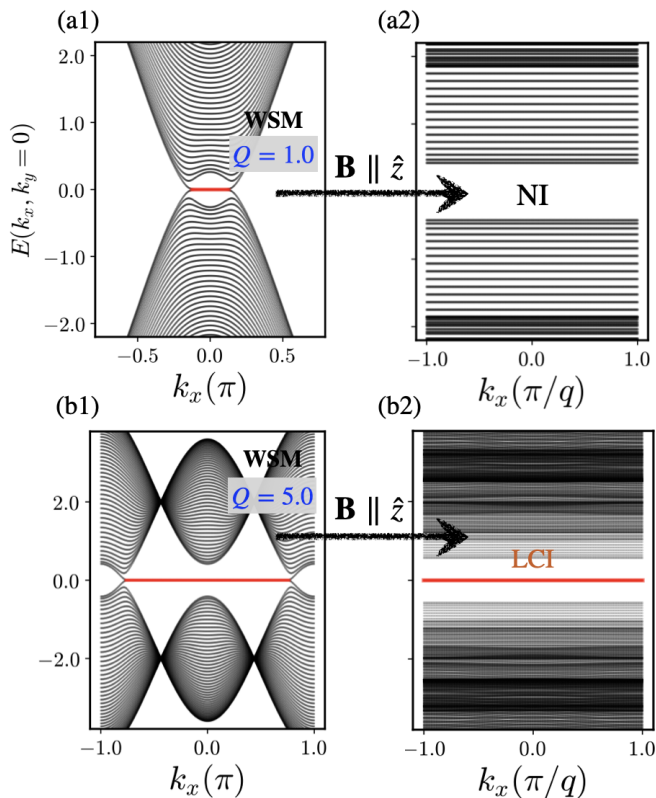


FIG. 4. Energy spectrum (along k_x) in a slab geometry along z direction with thickness $L_z = 50$ in units of lattice constant for $\gamma \approx -0.30$ (negative). Energies are given in units of v_x . Left column shows the slab spectrum for zero field, highlighting the zero energy Fermi-arc surface states (a1) for small ($Q = 1$) and (b1) large ($Q = 5$) separation between the Weyl nodes. Right column shows the slab spectrum in presence of an external field applied along z direction corresponding to a flux of $\phi_B/\phi_0 = 1/q$ with $q = 10$. (a2) Fermi-arc states get fully gapped out (NI phase). (b2) The Fermi-arc states of the WSM evolve to the surface states of a LCI phase (highlighted in red). The surface states in the LCI phase are extended to the edge of the magnetic BZ along k_x .

in the absence of a magnetic field. Then, one can introduce the k_x -dependent Chern number $C(k_x)$, which measures the Chern number in the k_y - k_z plane at fixed k_x of the occupied bands. For the lattice model defined in Eq. 1, $\sum_{n \in occ} C_n(k_x) = 1$ for all values of k_x in between the two Weyl nodes, $-k_0 < k_x < k_0$, and it is zero otherwise. For a system in a slab geometry with a surface in the xy plane, this gives rise to Fermi arc states on the surface connecting the projection of the two Weyl nodes on the k_x - k_y surface BZ.

We now consider the effect of a magnetic field. When the two WNs are close to the center of the BZ, the Fermi arcs are short (see Fig. 4(a1)). We then intuitively expect the WNs to gap out due to Q tunneling (tunneling within the first BZ), and the Fermi arcs to disappear in the presence of a magnetic field [43]. This corresponds to a topologically trivial insulating phase, which we refer to

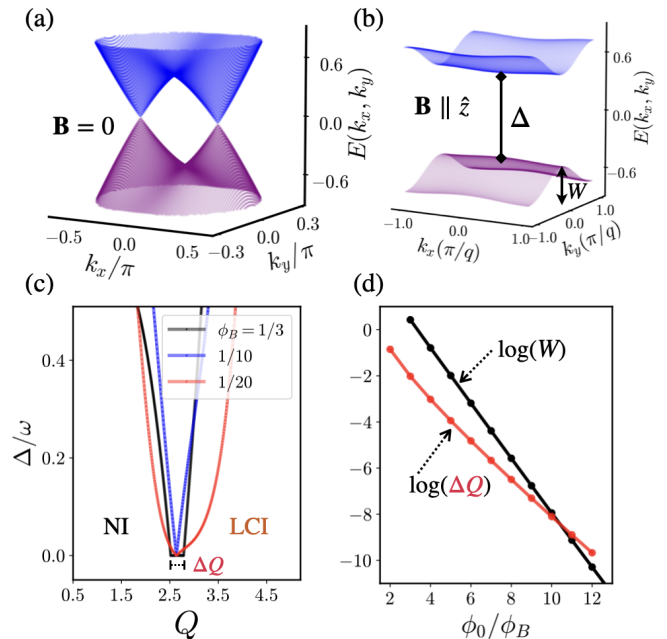


FIG. 5. Behavior of the gap for $\gamma < 0$. (a) Zero field energy spectrum is showing two Weyl cones separated along k_x . (b) In presence of an orbital $\mathbf{B} \parallel \hat{z}$, Weyl cones are gapped out. Only two Landau bands near zero energy are shown. For flux $\phi_B \sim \phi_0$, the bands have a finite bandwidth (W). (c) Energy gap (Δ) as a function of Weyl nodes' separation for flux values $\phi_B/\phi_0 = 1/q = 1/3, 1/10, 1/20$. Magnetic field immediately creates a gap in the spectrum for almost any value of separation between the Weyl nodes. The gap is exponentially small $\sim \exp(-Q^2 l_B^2)$. For intermediate values of separation, WSM state survives but in an exponentially small vicinity of k_0 (seen most clearly for $\phi_B/\phi_0 = 1/3$). (d) The width of the gapless region (denoted by ΔQ in (c)) where the system remains in the WSM phase falls exponentially with ϕ_B^{-1} . The bandwidth (denoted as W in (b)) also falls as $\exp(-\phi_B^{-1})$.

as normal insulator (NI).

On the other hand, when the Weyl nodes approach each other across the edges of the BZ, the Fermi arcs are long, nearly spanning the full BZ in the k_x direction (see Fig. 4(b1)). Now, when we apply a magnetic field, we expect the Weyl nodes to gap out due to Q' tunneling (tunneling across the edge of the BZ), but the gapless Fermi arc states to survive [43]. This corresponds to the LCI phase.

We note that this behavior is expected independently of the sign of γ . These notions can be made more concrete by introducing the magnetic BZ, which we discuss next. In the magnetic BZ, the momenta are good quantum numbers, making it possible to track the evolution of the Weyl nodes and Fermi arcs in the presence of a magnetic field. Figure 4(a2,b2) shows the spectrum on the magnetic BZ for the Q and Q' tunneling cases, respectively, where the NI and LCI phases are observed. These results will be discussed in more detail below. Interestingly, the more careful analysis will also reveal the ap-

pearance of an additional gapped insulating phase, LCI', which alternates with the NI phase in the case $\gamma > 0$.

As shown in this section, the behavior of the Fermi-arc surface states discussed above in the presence of a magnetic field is consistent with the nonperturbative gap-opening mechanism in the bulk Weyl semimetal. Fermi-arc states with a short arc length disappear once the magnetic field is applied. In this regime, the surface states acquire a finite lifetime, as electrons initially localized at the surface can escape into the bulk through chiral Landau levels. This fate of short Fermi arcs has also been predicted in a recent continuum analysis [53]. In contrast, Fermi-arc states with a long arc length persist and smoothly evolve into the chiral surface states of the LCI phase.

A. Bloch-Hofstadter Hamiltonian

In what follows we will set $t = 1$ in our lattice model. In presence of an orbital magnetic field along z direction (i.e. perpendicular to the direction of separation \vec{Q}), and using the Landau gauge $\mathbf{A} = (-y, 0, 0)B$, the Hamiltonian in Eq. 1 takes the following form

$$H_\phi = \sum_y \sum_{k_x, k_z} c_y^\dagger 2[f_1(y)\sigma_x + f_2(y)\sigma_z]c_y - \left(c_{y+1}^\dagger (\tilde{v}_x\sigma_x + iv_y\sigma_y) c_y + H.c \right). \quad (9)$$

Here $f_1(y) = \tilde{v}_x(2 + \cos(k_0 a) - \cos(k_z a) - \cos(k_x a + 2\pi\phi_B y))$, $f_2(y) = f_2 = v_z \sin(k_z a)$, and $\phi_B = Ba^2/\phi_0$ ($\phi_0 = h/e$) is the magnetic flux through a 2D unit cell in the x - y plane. Unless otherwise stated, hereafter we set $v_x = 1$ and vary v_y to control γ .

Translation symmetry can be restored when the flux is commensurate with the lattice. This is done by choosing an enlarged unit cell containing an integer number of flux quanta. In what follows we will choose commensurate flux $\phi_B/\phi_0 = p/q$, where q is a positive integer and without loss of generality we will set $p = 1$ throughout this paper. The enlarged unit cell is then obtained by extending the original unit cell q times along the y direction. This gives a magnetic BZ with $-\pi \leq k_x a \leq \pi$, $-\pi/q \leq k_y a \leq \pi/q$, $-\pi \leq k_z a \leq \pi$. Working with the magnetic BZ will allow us to compute topological invariants and track the evolution of the Fermi arc states in a straightforward manner. Although k_x in the magnetic BZ lies in the range $(-\pi, \pi)$ the spectrum along k_x is in fact periodic with a period of $2\pi/q$ [54]. Therefore, in the analysis below we restrict ourselves to $k_x \in (-\pi/q, \pi/q)$.

Here we emphasize that, in contrast to Landau levels in the continuum, the Hofstadter Bloch bands arising at commensurate magnetic flux can host Weyl nodes and carry nonzero Chern numbers. Throughout this work, when we refer to a WSM phase in the presence of a magnetic field, we specifically mean that the corresponding Hofstadter Bloch bands exhibit Weyl nodes pinned at

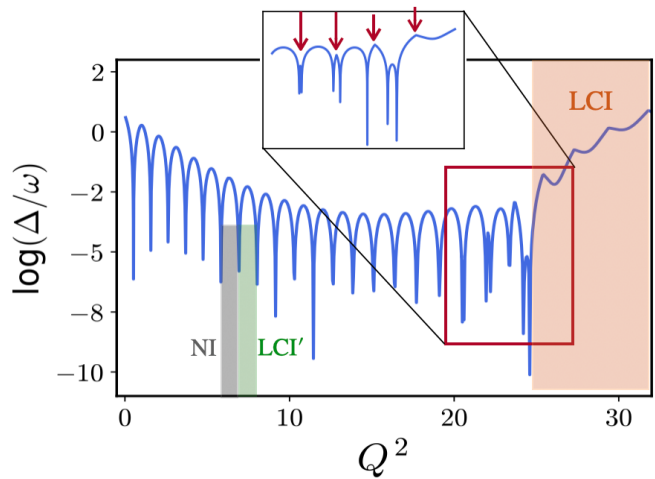


FIG. 6. Logarithm of the energy gap Δ as a function of the square of the separation between the Weyl nodes for a fixed flux $\phi_B/\phi_0 = 1/50$, and for $\gamma = 0.96$ (positive). The troughs are not exactly at zero because of a numerical artifact: finite sampling for Q as well as for momenta. Periodic closing of gap stops after a certain value of $Q^2 \approx 24$. Near that value, besides the smooth peaks, we observe additional sharp peaks (shown in the inset). For $Q \gtrsim 24$, the system is in an LCI state. For $Q \lesssim 24$, the WSM under magnetic field alternates between an NI and an LCI' which can be viewed as two copies of an LCI with opposite Chern numbers.

zero energy.

B. Phase diagram for $\gamma < 0$

For the special case $\tilde{v}_x = v_y = 1$, we can understand the transition between NI and LCI analytically by solving for the zeros of the Bloch-Hofstadter Hamiltonian in Eq. 9. These correspond to Weyl nodes in the magnetic BZ [42, 43], and their appearance is determined by the condition

$$\cos qk_x = T_q(g) - 2^{q-1}, \quad (10)$$

where $T_q(g)$ is Chebyshev polynomial of the first kind of degree $q = \phi_0/\phi_B$, and $g = 1 + \cos k_0$. Since $0 \leq k_0 \leq \pi$, the parameter g lies in the range $0 \leq g \leq 2$.

Equation (10) determines when the WSM under magnetic field becomes gapped or remains gapless. For certain values of q and g , the equation has no solutions, which indicates a gapped phase. On the other hand, if the right-hand-side of the equation lies in the range $(-1, 1)$, then there are real solutions, indicating that the spectrum contains two WNs at $(\pm k_1, 0, 0)$, where $0 < k_1 < \pi/q$ is the solution for k_x in Eq. (10).

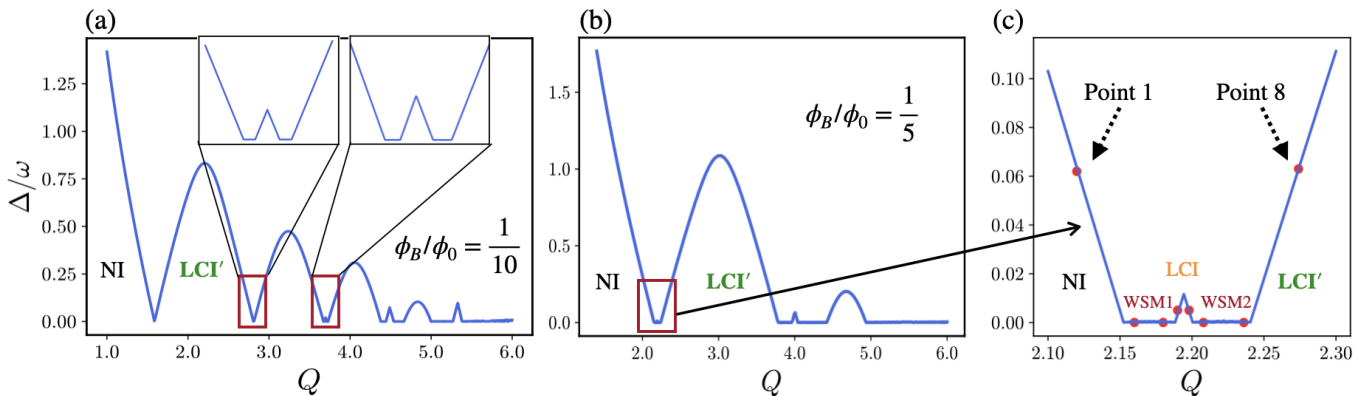


FIG. 7. Energy gap as a function of separation between the Weyl nodes for sizable fluxes (a) $\phi_B/\phi_0 = 1/10$ and (b) $\phi_B/\phi_0 = 1/5$ for a fixed $\gamma = 0.96$. See text for a detailed discussion of the sequence and structure of the transitions between the different gapped phases. (c) In a transition from an NI to an LCI' the system goes through several closings and reopenings of the gap, as shown in Fig. 8. The red dots in (c) correspond to the values of Q at which the energy bands in Fig. 8 are plotted.

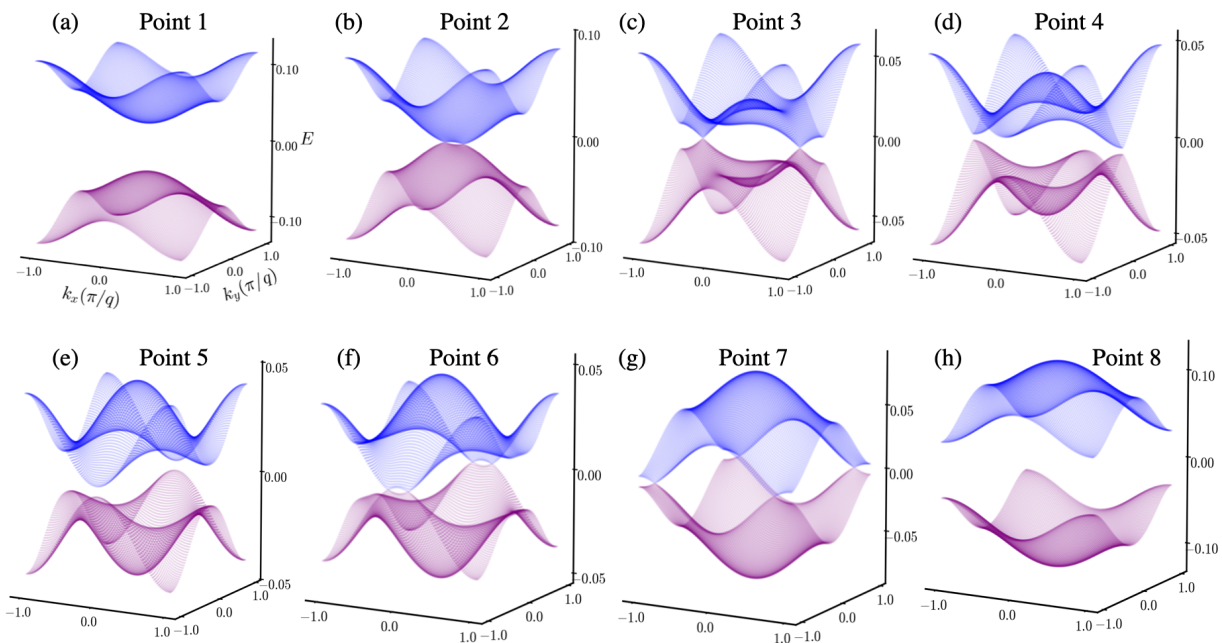


FIG. 8. Gap closing, formation of Weyl cones, and gap reopening across the transition between the NI and LCI' states, as Q is increased, shown in Fig. 7(c). Here the flux is fixed and equal to $\phi_B/\phi_0 = 1/5$. The values of Q at which the energy bands are plotted are indicated by red dots in Fig. 7(c). The transition from (a) to (d) involves a band inversion at $(0,0)$, and the transition from (e) to (h) involves another band inversion at $(\pi/q, \pi/q)$.

Consider first the limit of large q , corresponding to a small flux. In this limit, 2^{q-1} is exponentially large and we can neglect the cosine term by comparison. Then,

$$T_q(g) \approx 2^{q-1}. \quad (11)$$

Since $-1 < T_q(g) < 1$ for $g \leq 1$, the above equation can admit a solution only when $g > 1$. For $g > 1$, we have $2T_q(g) = 2 \cosh(q \cosh^{-1}(g)) = \exp(q \ln(g + \sqrt{g^2 - 1})) + \exp(-q \ln(g + \sqrt{g^2 - 1}))$. Substituting this expression of $T_q(g)$ we convert the above condition into a quadratic equation. This equa-

tion admits a single solution, $g = 5/4$. Thus, in the limit of large q , the system is gapped for all values of $Q = 2k_0$ except for $Q^* = 2k_0^* = 2 \cos^{-1}(1/4)$.

Reintroducing the cosine results in a finite range of g where the system is gapless, $g_1 < g < g_2$, where g_1 and g_2 are critical values surrounding $g = 5/4$. This corresponds to the WSM phase that separates the two insulating states. The width of this region $g_2 - g_1$ is of order 2^{-q} , i.e. it is exponentially small in $1/\phi_B$, as shown in Fig. 5(e).

To understand the topological nature of the gapped phases, we calculate the k_x -dependent Chern number

$C(k_x)$ in the magnetic BZ. We find that for large g (i.e. small $Q < Q^*$) $\sum_{n \in occ} C_n(k_x) = 0$ for all k_x , corresponding to an NI. On the other hand, for small g (i.e. large $Q > Q^*$), $\sum_{n \in occ} C_n(k_x) = 1$ for all k_x , corresponding to an LCI phase. The transition between NI and LCI can be understood from the evolution of the solutions to Eq. (10). Let us fix the flux $1/q$ and look for solutions as g (or equivalently Q) is varied. Starting from large g (NI phase), when g is decreased to g_2 , the band gap closes and a Dirac point appears at the Gamma point of the magnetic BZ. Decreasing g further leads to a splitting of the Dirac point into a pair of WNs that move away from each other towards the zone boundary. In this regime, solving in the slab geometry, a Fermi arc appears at the surface, and its length increases with the separation between the WNs. At a second critical value, $g = g_1$, the two WNs merge at the edge of the magnetic BZ ($\pm\pi/q, 0, 0$) and disappear but the Fermi arc survives and spans the full magnetic BZ along k_x . Thus an LCI state emerges. This is demonstrated in Fig. 4.

Even though the exact solution above was derived for $\tilde{v}_x = v_y = 1$, we confirm that this behavior is generic for all $\gamma < 0$ by numerically solving the Bloch-Hofstadter Hamiltonian, Eq. (9). This is demonstrated in Fig. 5. We note that the finite width of the WSM phase can be attributed to the finite bandwidth of the Landau levels on a lattice. The width of the gapless region and the bandwidth are plotted in Fig. 5(e,f). As can be seen, they both show an exponential dependence $\sim \exp(-\phi_B^{-1})$.

C. Phase diagram for $\gamma > 0$ and appearance of LCI'

We now turn to $\gamma > 0$. Recall that in the continuum picture, closings and reopenings of the gap occur in an oscillatory fashion as either Q or the flux ϕ_B is varied. As discussed in Sec. III D, this can be understood from the semiclassical picture of destructive interference between two (intra-BZ) tunneling paths. On the lattice, there is an additional tunneling path available, inter-BZ tunneling. As the WNs approach the BZ edge, inter-BZ tunneling becomes dominant. Therefore, for large Q we expect the oscillations in the gap to stop and the system to enter an LCI phase. Furthermore, the inter-BZ tunneling affects the structure of the gap even for small Q , where the oscillations are no longer strictly periodic. This is demonstrated in Fig. 6.

In addition, as we'll show below, the gapped phases alternate between NI and a symmetry-protected topological phase, denoted LCI', as shown in Fig. 6. We expect the gap closing points between these phases to broaden into finite regions due to the finite bandwidth of the LLs, as observed for $\gamma < 0$. However, in this case, each transition exhibits a richer structure, with two WSM regions and an LCI phase in between, as shown in Fig. 7.

To understand the transition from NI to LCI', let us begin from the NI phase at small Q . As we approach the transition with increasing Q , two LL bands approach

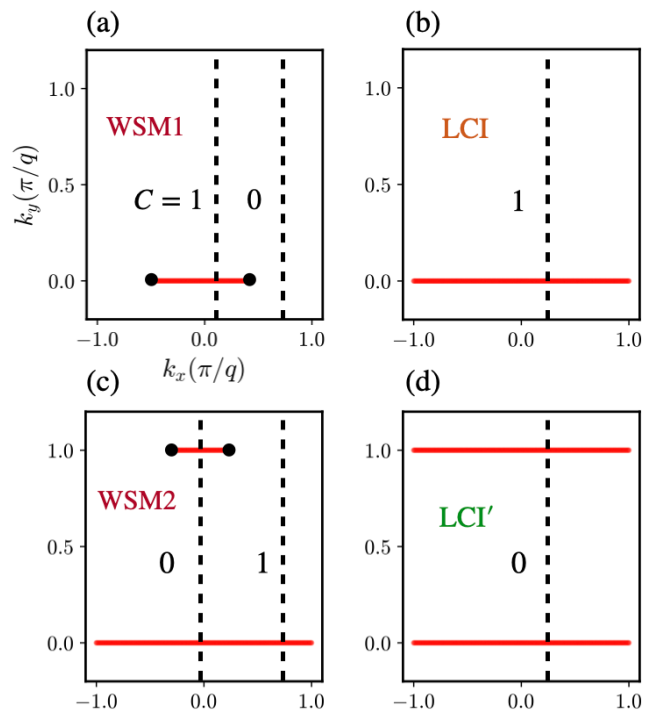


FIG. 9. Evolution of zero energy surface states in the k_x - k_y surface BZ in the transitions from an NI to an LCI' state (the transition is depicted in Fig. 7(c)) for a fixed flux $1/5$ and $\gamma = 0.96$. The Q values are 2.175, 2.195, 2.22 and 2.30 in (a)-(d) respectively. Figure (a) shows the zero energy Fermi-arc states of the WSM state which appear in the transition NI to LCI. Chern numbers are calculated for a fixed k_x value, indicated as vertical dashed lines representing (k_y, k_x) planes over which we integrate the Berry curvature. (b) As Q is increased, the Weyl nodes approach the edge of the magnetic BZ, merge, and get annihilated. At the end of this process, the corresponding Fermi arc spans the entire BZ along k_x . Thus an LCI state emerges. (c) A pair of Weyl nodes appear, accompanied by a new Fermi arc. This Fermi arc coexists with the surface states of the LCI bands. (d) As Q is increased further, the Weyl nodes approach the edge of the magnetic BZ, merge at $(\pi/q, \pi/q)$, and get annihilated. Again, the corresponding Fermi arc now spans the entire BZ along k_x . Thus an LCI' state emerges. In this state $C(k_x) = 0$ for all k_x .

each other (panel (a) of Fig. 8). We enter a WSM phase when the two bands touch at the Γ point of the magnetic BZ. Then, two WNs form and they move away from each other as we keep increasing Q (panels (b) and (c)). When the WNs reach the edge of the magnetic BZ, we enter an LCI phase (panel (d)). Increasing Q further, we enter another WSM phase when the two bands touch again, but this time at $(k_x, k_y) = (0, \pi/q)$. These WNs move away from each other (panels (f) and (g)) until they reach the corner of the magnetic BZ, when the system enters the LCI' phase (panel (h)). This entire sequence is reversed at the next gap closing, when the system evolves from LCI' to NI.

Note that the appearance of the LCI phase requires the gap at $(0, \pi/q)$ to be larger than that at $(\pi/q, 0)$. For the model we consider, this is always satisfied for $\gamma > 0$. This order of the gaps guarantees that the pair of WNs at $k_y = 0$ leaves the zone edge before the pair at $k_y = \pi/q$ is created. If the order were reversed, then the two pairs would coexist and a single WSM phase would separate the NI and LCI' phases.

The evolution of the Fermi arcs on a slab geometry is shown in Fig. 9. There, we see that the LCI phase is characterized by a closed Fermi arc that extends across the magnetic BZ. By contrast, the LCI' phase contains two such Fermi arcs, one along $k_y = 0$ and the other along $k_y = \pi/q$. These arcs have opposite chirality, such that the layer Chern number is zero. However, the LCI' is protected by mirror symmetry, which ensures that the Fermi arcs reside at the mirror symmetric values $k_y = 0$ or $k_y = \pi/q$, thus preventing them from merging and forming an NI. In the absence of mirror symmetry, there is no topological distinction between LCI' and NI. This is consistent with the observation made earlier, that gap closings are only expected in mirror symmetric models, due to the exact destructive interference between tunneling paths.

V. SUMMARY AND CONCLUSION

An external orbital magnetic field, which is perpendicular to the direction of separation of Weyl cones of opposite chirality, introduces tunneling of electrons between the Weyl cones. This leads to a hybridization between the cones (note that such a hybridization is allowed since translation symmetry is broken by the presence of the orbital magnetic field) and an opening of a gap. Such a tunneling process requires overcoming the energy barrier separating the two Weyl nodes, leading to a nonperturbative dependence of the gap on the magnetic field. The induced gap is significant when the inverse magnetic length is comparable to or larger than the momentum-space separation between the Weyl nodes.

Anisotropy in the Weyl cone dispersion, characterized by γ as defined in Eq. (2), plays a crucial role in determining the behavior of the induced gap. When $\gamma < 0$, the system enters either a normal insulator or an LCI phase, with the induced gap increasing monotonically as the magnetic field strength grows. In contrast, for $\gamma > 0$ and small Weyl node separation ($Q \ll \pi$), the gap exhibits periodic closings as the field increases, causing the system to alternate between a normal insulator and a gapped phase labeled LCI', which can be viewed as two copies of LCI with opposite Chern numbers. For $\gamma > 0$ and large node separation, the system enters directly into an LCI state.

Throughout, we assumed that the magnetic field is applied along the z axis. Then, the anisotropy parameter γ depends on the ratio of the velocity components of the

Weyl fermions v_y/v_x . An identical analysis can be carried out for a field applied along the y axis. Then, the relevant anisotropy parameter depends on the ratio v_z/v_x . For layered materials, where these two ratios can be very different, this opens the possibility to observe $\gamma > 0$ and $\gamma < 0$ behaviors on the same system by rotating the direction of the magnetic field, and to access the different induced phases, namely LCI, LCI' or a normal insulator.

We now turn to discuss briefly some of the experimental implications of our results. The magnetic field-induced gap opening in WSMs has direct consequences on the longitudinal magnetoresistance [41]. Such behavior has been already observed in experiments in the Weyl materials TaAs [36] and TaP [37]. However, longitudinal magnetoresistance does not give a direct indication of the topology of the gapped phases. In contrast, Hall conductivity measurements provide a clearer distinction between the gapped phases, namely the normal insulator, LCI, and LCI' phases. A time-reversal symmetry-breaking Weyl semimetal with two Weyl nodes separated by a momentum space distance Q along k_x exhibits a non-quantized anomalous Hall conductivity of $\sigma_{yz} = \frac{e^2}{2\pi h} Q$ per layer along the x -direction. Upon entering the LCI phase with applied magnetic field, this Hall conductivity becomes quantized at $\sigma_{yz} = \frac{e^2}{h}$ per layer. In contrast, transitions to either a normal insulator or the LCI' phase result in a vanishing Hall conductivity. To further distinguish between normal insulator and LCI', one may rely on surface-sensitive probes, such as STM, that can detect the presence of the zero-energy modes arising from the closed Fermi arc states in LCI'.

We briefly comment on the effects of disorder, finite temperature, and interactions on the phase diagram. In the presence of disorder, the LCI' phase cannot be sharply distinguished from a normal insulator, since the crystalline symmetry protecting the LCI' phase is generically broken. Moreover, features associated with exponentially small gaps and with very narrow regions in parameter space are expected to be smeared out by disorder and thermal fluctuations. Nevertheless, the phase transitions from the WSM to either a normal insulating phase or an LCI phase are expected to remain robust, provided that disorder, temperature, and interaction scales are small compared to the magnetic-field-induced gap.

Finally, we comment on orbital magnetic fields that are not perfectly perpendicular to the separation of the Weyl nodes. The momentum parallel to the magnetic field, $k_{\parallel B}$, is a good quantum number. When the field has a component parallel to the separation between Weyl nodes, the value of $k_{\parallel B}$ differs at the two Weyl nodes, and they no longer hybridize directly. Hence, even a small misalignment of the field relative to the perpendicular direction can drastically suppress the gap opening [41]. However, this effect is mitigated in systems with nodal loops [55–62]. In such systems, magnetic fields generically lead to direct hybridization of nodal states, regardless of the magnetic field orientation. This will be discussed in detail elsewhere.

ACKNOWLEDGMENTS

F.A. thanks the Helen Diller Quantum centre for financial support. A.K. acknowledges funding by the Israeli

Council for Higher Education support program and by the Israel Science Foundation (Grant No. 2443/22). D.P. acknowledges support from the Israel Science Foundation (ISF) Grant no. 2005/23.

-
- [1] S. Murakami, Phase transition between the quantum spin hall and insulator phases in 3d: emergence of a topological gapless phase, *New Journal of Physics* **9**, 356 (2007).
- [2] X. Wan, A. M. Turner, A. Vishwanath, and S. Y. Savrasov, Topological semimetal and fermi-arc surface states in the electronic structure of pyrochlore iridates, *Phys. Rev. B* **83**, 205101 (2011).
- [3] B. Q. Lv, H. M. Weng, B. B. Fu, X. P. Wang, H. Miao, J. Ma, P. Richard, X. C. Huang, L. X. Zhao, G. F. Chen, Z. Fang, X. Dai, T. Qian, and H. Ding, Experimental discovery of weyl semimetal taas, *Phys. Rev. X* **5**, 031013 (2015).
- [4] B. Q. Lv, N. Xu, H. M. Weng, J. Z. Ma, P. Richard, X. C. Huang, L. X. Zhao, G. F. Chen, C. E. Matt, F. Bisti, V. N. Strocov, J. Mesot, Z. Fang, X. Dai, T. Qian, M. Shi, and H. Ding, Observation of weyl nodes in taas, *Nature Physics* **11**, 724 (2015).
- [5] S.-Y. Xu, I. Belopolski, N. Alidoust, M. Neupane, G. Bian, C. Zhang, R. Sankar, G. Chang, Z. Yuan, C.-C. Lee, S.-M. Huang, H. Zheng, J. Ma, D. S. Sanchez, B. Wang, A. Bansil, F. Chou, P. P. Shibayev, H. Lin, S. Jia, and M. Z. Hasan, Discovery of a weyl fermion semimetal and topological fermi arcs, *Science* **349**, 613 (2015), <https://science.sciencemag.org/content/349/6248/613.full.pdf>
- [6] S.-Y. Xu, N. Alidoust, I. Belopolski, Z. Yuan, G. Bian, T.-R. Chang, H. Zheng, V. N. Strocov, D. S. Sanchez, G. Chang, C. Zhang, D. Mou, Y. Wu, L. Huang, C.-C. Lee, S.-M. Huang, B. Wang, A. Bansil, H.-T. Jeng, T. Neupert, A. Kaminski, H. Lin, S. Jia, and M. Zahid Hasan, Discovery of a weyl fermion state with fermi arcs in niobium arsenide, *Nature Physics* **11**, 748 (2015).
- [7] L. Lu, Z. Wang, D. Ye, L. Ran, L. Fu, J. D. Joannopoulos, and M. Soljačić, Experimental observation of weyl points, *Science* **349**, 622 (2015), <https://science.sciencemag.org/content/349/6248/622.full.pdf>.
- [8] H. Nielsen and M. Ninomiya, The Adler-Bell-Jackiw anomaly and weyl fermions in a crystal, *Physics Letters B* **130**, 389 (1983).
- [9] T. D. C. Bevan, A. J. Manninen, J. B. Cook, J. R. Hook, H. E. Hall, T. Vachaspati, and G. E. Volovik, Momentum creation by vortices in superfluid ^3He as a model of primordial baryogenesis, *Nature* **386**, 689 (1997).
- [10] V. Aji, Adler-Bell-Jackiw anomaly in Weyl semimetals: Application to pyrochlore iridates, *Phys. Rev. B* **85**, 241101 (2012).
- [11] A. A. Zyuzin and A. A. Burkov, Topological response in Weyl semimetals and the chiral anomaly, *Phys. Rev. B* **86**, 115133 (2012).
- [12] D. T. Son and B. Z. Spivak, Chiral anomaly and classical negative magnetoresistance of weyl metals, *Phys. Rev. B* **88**, 104412 (2013).
- [13] E. V. Gorbar, V. A. Miransky, and I. A. Shovkovy, Chiral anomaly, dimensional reduction, and magnetoresistivity of Weyl and Dirac semimetals, *Phys. Rev. B* **89**, 085126 (2014).
- [14] A. A. Burkov, Negative longitudinal magnetoresistance in Dirac and Weyl metals, *Phys. Rev. B* **91**, 245157 (2015).
- [15] P. Goswami, J. H. Pixley, and S. Das Sarma, Axial anomaly and longitudinal magnetoresistance of a generic three-dimensional metal, *Phys. Rev. B* **92**, 075205 (2015).
- [16] X. Huang, L. Zhao, Y. Long, P. Wang, D. Chen, Z. Yang, H. Liang, M. Xue, H. Weng, Z. Fang, X. Dai, and G. Chen, Observation of the chiral-anomaly-induced negative magnetoresistance in 3d weyl semimetal taas, *Phys. Rev. X* **5**, 031023 (2015).
- [17] C.-L. Zhang, S.-Y. Xu, I. Belopolski, Z. Yuan, Z. Lin, B. Tong, G. Bian, N. Alidoust, C.-C. Lee, S.-M. Huang, T.-R. Chang, G. Chang, C.-H. Hsu, H.-T. Jeng, M. Neupane, D. S. Sanchez, H. Zheng, J. Wang, H. Lin, C. Zhang, H.-Z. Lu, S.-Q. Shen, T. Neupert, M. Zahid Hasan, and S. Jia, Signatures of the Adler-Bell-Jackiw chiral anomaly in a weyl fermion semimetal, *Nature Communications* **7**, 10735 (2016).
- [18] X. Li, B. Roy, and S. Das Sarma, Weyl fermions with arbitrary monopoles in magnetic fields: Landau levels, longitudinal magnetotransport, and density-wave ordering, *Phys. Rev. B* **94**, 195144 (2016).
- [19] H.-Z. Lu and S.-Q. Shen, Quantum transport in topological semimetals under magnetic fields, *Frontiers of Physics* **12**, 127201 (2017).
- [20] S. Nandy, G. Sharma, A. Taraphder, and S. Tewari, Chiral anomaly as the origin of the planar hall effect in weyl semimetals, *Phys. Rev. Lett.* **119**, 176804 (2017).
- [21] H. Li, H.-W. Wang, H. He, J. Wang, and S.-Q. Shen, Giant anisotropic magnetoresistance and planar Hall effect in the Dirac semimetal Cd_3As_2 , *Phys. Rev. B* **97**, 201110 (2018).
- [22] Shama, R. Gopal, and Y. Singh, Observation of planar hall effect in the ferromagnetic weyl semimetal $\text{Co}_3\text{Sn}_2\text{S}_2$, *Journal of Magnetism and Magnetic Materials* **502**, 166547 (2020).
- [23] L. Li, J. Cao, C. Cui, Z.-M. Yu, and Y. Yao, Planar hall effect in topological weyl and nodal-line semimetals, *Phys. Rev. B* **108**, 085120 (2023).
- [24] Y.-W. Wei, J. Feng, and H. Weng, Spatial symmetry modulation of planar hall effect in weyl semimetals, *Phys. Rev. B* **107**, 075131 (2023).
- [25] A. C. Potter, I. Kimchi, and A. Vishwanath, Quantum oscillations from surface fermi arcs in weyl and dirac semimetals, *Nature Communications* **5**, 5161 (2014).
- [26] Y. Zhang, D. Bulmash, P. Hosur, A. C. Potter, and A. Vishwanath, Quantum oscillations from generic surface fermi arcs and bulk chiral modes in weyl semimetals, *Scientific Reports* **6**, 23741 (2016).
- [27] P. J. W. Moll, N. L. Nair, T. Helm, A. C. Potter, I. Kimchi, A. Vishwanath, and J. G. Analytis, Transport evidence for fermi-arc-mediated chirality transfer in the dirac semimetal Cd_3As_2 , *Nature* **535**, 266 (2016).

- [28] C. M. Wang, H.-P. Sun, H.-Z. Lu, and X. C. Xie, 3d quantum hall effect of fermi arcs in topological semimetals, *Phys. Rev. Lett.* **119**, 136806 (2017).
- [29] C. Zhang, Y. Zhang, X. Yuan, S. Lu, J. Zhang, A. Narayan, Y. Liu, H. Zhang, Z. Ni, R. Liu, E. S. Choi, A. Suslov, S. Sanvito, L. Pi, H.-Z. Lu, A. C. Potter, and F. Xiu, Quantum hall effect based on weyl orbits in cd3as_2 , *Nature* **565**, 331 (2019).
- [30] H. Li, H. Liu, H. Jiang, and X. C. Xie, 3d quantum hall effect and a global picture of edge states in weyl semimetals, *Phys. Rev. Lett.* **125**, 036602 (2020).
- [31] M. Chang, H. Geng, L. Sheng, and D. Y. Xing, Three-dimensional quantum hall effect in weyl semimetals, *Phys. Rev. B* **103**, 245434 (2021).
- [32] R. Ma, D. N. Sheng, and L. Sheng, Three-dimensional quantum hall effect and magnetothermoelectric properties in weyl semimetals, *Phys. Rev. B* **104**, 075425 (2021).
- [33] M. Chang, Y. Ge, and L. Sheng, Generalization of the theory of three-dimensional quantum hall effect of fermi arcs in weyl semimetal, *Chinese Physics B* **31**, 057304 (2022).
- [34] X.-X. Zhang and N. Nagaosa, Anisotropic three-dimensional quantum hall effect and magnetotransport in mesoscopic weyl semimetals, *Nano Letters* **22**, 3033 (2022), pMID: 35332773, <https://doi.org/10.1021/acs.nanolett.2c00296>.
- [35] G. Montambaux, F. Piéchon, J.-N. Fuchs, and M. O. Goerbig, Merging of dirac points in a two-dimensional crystal, *Phys. Rev. B* **80**, 153412 (2009).
- [36] C.-L. Zhang, S.-Y. Xu, C. M. Wang, Z. Lin, Z. Z. Du, C. Guo, C.-C. Lee, H. Lu, Y. Feng, S.-M. Huang, G. Chang, C.-H. Hsu, H. Liu, H. Lin, L. Li, C. Zhang, J. Zhang, X.-C. Xie, T. Neupert, M. Z. Hasan, H.-Z. Lu, J. Wang, and S. Jia, Magnetic-tunnelling-induced weyl node annihilation in TaP , *Nature Physics* **13**, 979 (2017).
- [37] B. J. Ramshaw, K. A. Modic, A. Shekhter, Y. Zhang, E.-A. Kim, P. J. W. Moll, M. D. Bachmann, M. K. Chan, J. B. Betts, F. Balakirev, A. Migliori, N. J. Ghimire, E. D. Bauer, F. Ronning, and R. D. McDonald, Quantum limit transport and destruction of the weyl nodes in TaAs , *Nature Communications* **9**, 2217 (2018).
- [38] C.-K. Chan and P. A. Lee, Emergence of gapped bulk and metallic side walls in the zeroth Landau level in dirac and weyl semimetals, *Phys. Rev. B* **96**, 195143 (2017).
- [39] P. Kim, J. H. Ryoo, and C.-H. Park, Breakdown of the chiral anomaly in weyl semimetals in a strong magnetic field, *Phys. Rev. Lett.* **119**, 266401 (2017).
- [40] D. R. Saykin, K. S. Tikhonov, and Y. I. Rodionov, Landau levels with magnetic tunneling in a Weyl semimetal and magnetoconductance of a ballistic $p-n$ junction, *Phys. Rev. B* **97**, 041202 (2018).
- [41] G. Bednik, K. S. Tikhonov, and S. V. Syzranov, Magnetotransport and internodal tunnelling in weyl semimetals, *Phys. Rev. Res.* **2**, 023124 (2020).
- [42] F. Abdulla, A. Das, S. Rao, and G. Murthy, Time-reversal-broken Weyl semimetal in the Hofstadter regime, *SciPost Phys. Core* **5**, 014 (2022).
- [43] F. Abdulla, Pairwise annihilation of weyl nodes induced by magnetic fields in the hofstadter regime, *Phys. Rev. B* **109**, 155142 (2024).
- [44] T. Devakul, Y. H. Kwan, S. L. Sondhi, and S. A. Parameswaran, Quantum oscillations in the zeroth Landau level: Serpentine Landau fan and the chiral anomaly, *Phys. Rev. Lett.* **127**, 116602 (2021).
- [45] T. Wehling, A. Black-Schaffer, and A. Balatsky, Dirac materials, *Advances in Physics* **63**, 1 (2014), <https://doi.org/10.1080/00018732.2014.927109>.
- [46] A. H. Castro Neto, F. Guinea, N. M. R. Peres, K. S. Novoselov, and A. K. Geim, The electronic properties of graphene, *Rev. Mod. Phys.* **81**, 109 (2009).
- [47] M. I. Katsnelson, Graphene: carbon in two dimensions, *Materials Today* **10**, 20 (2007).
- [48] M. Z. Hasan and C. L. Kane, Colloquium: Topological insulators, *Rev. Mod. Phys.* **82**, 3045 (2010).
- [49] X.-L. Qi and S.-C. Zhang, Topological insulators and superconductors, *Rev. Mod. Phys.* **83**, 1057 (2011).
- [50] M. H. Cohen and L. M. Falicov, Magnetic breakdown in crystals, *Phys. Rev. Lett.* **7**, 231 (1961).
- [51] M. Kaganov and A. Slutskin, Coherent magnetic breakdown, *Physics Reports* **98**, 189 (1983).
- [52] D. Shoenberg, *Magnetic Oscillations in Metals*, Cambridge Monographs on Physics (Cambridge University Press, 1984).
- [53] T. Bauer, F. Bucchieri, A. De Martino, and R. Egger, Quantum description of fermi arcs in weyl semimetals in a magnetic field, *Phys. Rev. Res.* **6**, 043201 (2024).
- [54] B. A. Bernevig and T. L. Hughes, *Topological Insulators and Topological Superconductors*, student edition (Princeton University Press, 2013).
- [55] C. Fang, Y. Chen, H.-Y. Kee, and L. Fu, Topological nodal line semimetals with and without spin-orbital coupling, *Phys. Rev. B* **92**, 081201 (2015).
- [56] G. Bian, T.-R. Chang, R. Sankar, S.-Y. Xu, H. Zheng, T. Neupert, C.-K. Chiu, S.-M. Huang, G. Chang, I. Belopolski, D. S. Sanchez, M. Neupane, N. Alidoust, C. Liu, B. Wang, C.-C. Lee, H.-T. Jeng, C. Zhang, Z. Yuan, S. Jia, A. Bansil, F. Chou, H. Lin, and M. Z. Hasan, Topological nodal-line fermions in spin-orbit metal pb-tase_2 , *Nature Communications* **7**, 10556 (2016).
- [57] T. Bzdušek, Q. Wu, A. Rüegg, M. Sigrist, and A. A. Soluyanov, Nodal-chain metals, *Nature* **538**, 75 (2016).
- [58] M. Neupane, I. Belopolski, M. M. Hosen, D. S. Sanchez, R. Sankar, M. Szlowska, S.-Y. Xu, K. Dimitri, N. Dhakal, P. Maldonado, P. M. Oppeneer, D. Kaczorowski, F. Chou, M. Z. Hasan, and T. Durakiewicz, Observation of topological nodal fermion semimetal phase in ZrS_2 , *Phys. Rev. B* **93**, 201104 (2016).
- [59] R. Lou, P. Guo, M. Li, Q. Wang, Z. Liu, S. Sun, C. Li, X. Wu, Z. Wang, Z. Sun, D. Shen, Y. Huang, K. Liu, Z.-Y. Lu, H. Lei, H. Ding, and S. Wang, Experimental observation of bulk nodal lines and electronic surface states in ZrB_2 , *npj Quantum Materials* **3**, 10.1038/s41535-018-0121-4 (2018).
- [60] I. Belopolski, K. Manna, D. S. Sanchez, G. Chang, B. Ernst, J. Yin, S. S. Zhang, T. Cochran, N. Shumiya, H. Zheng, B. Singh, G. Bian, D. Multer, M. Litskevich, X. Zhou, S.-M. Huang, B. Wang, T.-R. Chang, S.-Y. Xu, A. Bansil, C. Felser, H. Lin, and M. Z. Hasan, Discovery of topological weyl fermion lines and drumhead surface states in a room temperature magnet, *Science* **365**, 1278 (2019).
- [61] F. Abdulla, G. Murthy, and A. Das, Internal symmetry protected stable topological semimetals in three dimensions, *Phys. Rev. B* **112**, 205111 (2025).
- [62] W. Chen, L. Liu, W. Yang, D. Chen, Z. Liu, Y. Huang, T. Zhang, H. Zhang, Z. Liu, and D. W. Shen, Evidence of topological nodal lines and surface states in the centrosymmetric superconductor SnTas_2 , *Phys. Rev. B* **103**,

035133 (2021).